Digital Object Identifier (DOI): 10.1109/IECON.2015.7392925

Industrial Electronics Society, IECON 2015 - 41st Annual Conference of the IEEE; November 2015

Active thermal control of IGBT power electronic converters

Johannes Falck
Markus Andresen
Marco Liserre

Suggested Citation

J. Falck, M. Andresen and M. Liserre, "Active thermal control of IGBT power electronic converters," *Industrial Electronics Society, IECON 2015 - 41st Annual Conference of the IEEE*, Yokohama, 2015, pp. 000001-000006.

Active Thermal Control of IGBT Power Electronic Converters

Johannes Falck, *Student Member, IEEE*, Markus Andresen, *Student Member, IEEE*, Marco Liserre, *Fellow, IEEE*
Chair of Power Electronics, Faculty of Engineering
Christian-Albrechts-Universität zu Kiel, Kaiserstr. 2, 24143 Kiel, Germany
Email: jofa@tf.uni-kiel.de, ma@tf.uni-kiel.de, ml@tf.uni-kiel.de

***Abstract*—Thermal cycling is one of the main sources of aging and failures in power electronics. A possibility to reduce the stress to semiconductors is to control the amount of losses that occur in the device during operation. This work presents an active thermal controller that aims at reducing the junction temperature variations in the case of variable power profile. The switching frequency of the converter is the parameter that is affected by the active thermal control, while the operation of the converter remains unchanged. The novelty of the approach is that the switching frequency variation is exploited to prevent excessive cooling down of the semiconductor during a power reduction. A thermal model is used to estimate the losses, so the prior knowledge of the mission profile is not needed. The results of the proposed solution are validated with an experimental prototype and a wide-bandwidth temperature measurement system directly applied to the semiconductor chip. Finally, the impacts of the controller on the module's lifetime is estimated.**

***Index Terms*—Power Electronics Reliability, Thermal Cycling, Junction Temperature Estimation, Lifetime Prediction, IGBT**

I. Introduction

Power electronics are employed in a multitude of applications, including grid feeding converters for renewable energy sources [1], inverters for electric vehicles and motor drives in industrial processes [2]. Reliability of power electronics is becoming an increasingly important factor in the system design [3], [4]. Power semiconductors in the lower and medium power range are often combined in modules to increase the power density and reduce the material consumption [5].

Power electronic modules consist of several material layers to maintain functionality and electric insulation [6]. For the electric connection between chips and terminals aluminum bondwires are usually used [7]. The schematic of an IGBT-module is shown in Fig. 1. Due to ambient temperature changes and alternating power consumption these layers experience ongoing heating and cooling processes, so called thermal cycles [8]. As the coefficients of thermal expansion (CTE) in the layers mismatch, mechanical stress is caused within the module [9], leading to aging and destruction of the modules [10]. The thermal cycle magnitude is the most critical parameter for the scale of the aging [11]. Especially short-term thermal cycling in the order of a second leads to fatigue of the bonds and therefore bondwire lift off. Long-term cycles can affect the temperature of the base plate despite of its high thermal capacitance and cause solder fatigue [12]. Failures

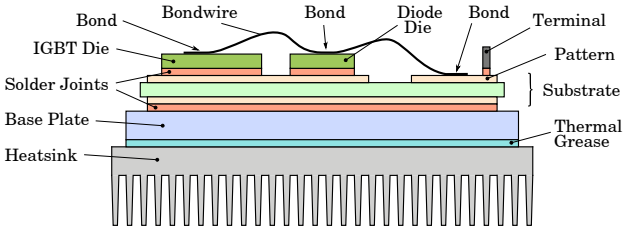

Fig. 1. Layer sequence of an IGBT-module connected to heatsink.

in the modules cause maintenance and replacement and thus downtimes and costs for the operators.

In order to increase lifetime and reliability of power electronic modules, improvements in the connection technology and assembly of the modules have been done. Sintering instead of soldering of the chips is used to increase strength of the connections [5]. The matching of CTE values and the heat dissipation performance is improved by the use of advanced materials [5], [8]. Delaminating of the substrate can be reduced by avoiding $90\,^{\circ}$ angles in the pattern [8]. Other strategies try to prevent thermal cycles from emerging in the module. Low-term ambient temperature swings can be addressed with regulated cooling [13]. A method that faces the much higher amount of short-term and medium-term thermal cycles is active thermal control.

Active thermal control uses temperature related control parameters to influence the junction temperatures online. The goal is to reduce the thermal stress in the module by smoothing the temperature variation. To influence the junction temperatures, the thermal control increases or decreases the losses in the desired chips temporary. Only few active thermal control approaches have been proposed so far. Chosen control parameters are the switching frequency [2], [14], the modulation method [15], the dc link voltage [16], the gate voltage [17] or circulating reactive power [18]. As an example, a short-term temperature drop can be prevented or reduced when losses are increased temporary by increasing the switching frequency. Active thermal control can be performed without knowledge of the junction temperature [19]. Also, an electro-thermal model can be used to achieve online estimations of the junction temperatures on the basis of electrical measurements to enable more precise control of the thermal stress [2].

This paper achieves a reduced thermal stress without interfering the system operation such as preventing switching

operations and thus adding current ripple [15] or limiting the maximal power [14]. Using the proposed thermal control, the applications operation points stay untouched, as only temporary increments of the switching frequency are performed. Furthermore, experimental validation of both, the online junction temperature estimation and thermal control in application-related mission profiles, has not yet been proposed. Thus, in this paper detailed experimental validation using a high-bandwidth temperature measurement is done for a crane application and an electric vehicle. Also, an estimation on the extension of the modules lifetime using the thermal control is done. It is based on the Coffin-Manson model [20] and Miner's rule for accumulated damage [9].

In the following a possibility to estimate junction temperatures online is given in Section II. Next, the active thermal control concept is represented in Section III. Experimental results are shown in Section IV. Finally, a conclusion is given in Section V.

II. Electro-Thermal Model

A real-time knowledge of the junction temperatures of a power module is of interest for active thermal control. Measurements of the junction temperatures are possible, but the necessary high-bandwidth sensors are expensive and only used in experimental setups. As high potential for lifetime extension is in elimination of short-term thermal cycles [11], usual thermocouples connected to the chips cannot fulfill the bandwidth demand. Thus, in commercial product solutions, junction temperature estimations on the basis of electrical measurements [21] are more realistic as there is no need to increase complexity of power modules. The electro-thermal model for this purpose consist of three parts: A device model that holds the electrical characteristics of the used power module, a power losses model for the semiconductors, and a thermal model to estimate the heat propagation in the module.

A. Losses model

In power electronic systems usually the switching losses and conduction losses are the dominant losses [5]. The conduction losses of an IGBT $P_{cond,igbt}$ are computed in dependency of the collector current i_c and the collector-emitter voltage v_{ce}. This voltage drop is substantially dependent on i_c, the junction temperature $T_{j,igbt}$ and the applied gate voltage v_{ge}.

$$P_{cond,igbt} = i_c \cdot v_{ce}(i_c, T_{j,igbt}, v_{ge}) \tag{1}$$

Conduction losses in power diodes $P_{cond,diode}$ have a similar structure. They are depend on the forward current i_f and its forward voltage v_f characteristic, which is dependent on i_f and the junction temperature $T_{j,diode}$.

$$P_{cond,diode} = i_f \cdot v_f(i_f, T_{j,diode}) \tag{2}$$

The characteristics of the chips are placed in look-up tables for online computation. As usually a large range of linear behavior is present, the look-up tables can be written compact.

The amount of switching losses in IGBTs $P_{sw,igbt}$ depends on the switching energies E_{on} and E_{off}, which depend mainly on i_c, v_{ce} and $T_{j,igbt}$. Manufacturers indicate the switching energies often for a specified operation point, so approximations have to be done for general calculation. A linear approximation for one fundamental period is given in [5], using the parameters of a given operating point i_{ref}, v_{ref}, $T_{j,igbt,ref}$ and scaling it to the desired operating point:

$$P_{sw,igbt} = f_{sw} \cdot (E_{on} + E_{off}) \frac{\sqrt{2}}{\pi} \frac{i_c}{i_{ref}} \left(\frac{v_{dc}}{v_{ref}} \right)^{K_v} \cdot (1 + c_{T,sw} (T_{j,igbt} - T_{j,igbt,ref})) \tag{3}$$

The parameters K_v and $c_{T,sw}$ are empirically determined constants set to $K_v = 1.35$ and $c_{T,sw} = 0.003$. In power diodes reverse recovery losses $P_{sw,diode}$ occur during switch-off and their amount depends on the recovery energy E_{rr}. Similar to the IGBT switching energies, an approximation is given:

$$P_{sw,diode} = f_{sw} \cdot E_{rr} \left(\frac{\sqrt{2}}{\pi} \frac{i_f}{i_{ref}} \right)^{K_i} \left(\frac{v_f}{v_{ref}} \right)^{K_v} \cdot (1 + c_{T,rr} (T_{j,diode} - T_{j,diode,ref})) \tag{4}$$

Again, the additional parameters K_i and $c_{T,rr}$ are empirically determined constants set to $K_i = 0.6$ and $c_{T,rr} = 0.006$. Anyway, these equations give only estimations of the switching losses, which could deviate from reality, especially when the system works far from the reference values.

B. Thermal model

A linear Cauer-type thermal network is used to describe the heat propagation in the power electronic system. Parameter values for the thermal resistances and capacities are given by the module's datasheet. A complete estimation of the temperatures from ambient to the junctions needs high computational effort. To decrease computation time for online temperature estimations, a low-bandwidth temperature sensor on the modules substrate is included into the model. A sensor like that is often build into commercial IGBT modules. The advantage is, that only the temperature difference between the substrate and the junctions need to be calculated. This makes the control independent from the cooling system and results in a smaller thermal network, having less computational effort compared to approaches using a heatsink or ambient temperature measurement. A drawback is that short-term cycles of substrate temperature cannot be detected. However, due to the thermal capacitance of the substrate these fast cycles are small compared to the junction temperature cycles.

A four-part thermal network is often used in datasheets to describe the transient from junction to case. This is shown in Fig. 2. To implement the thermal network on a control system,

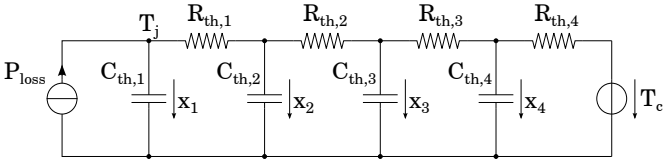

Fig. 2. Thermal network from junction to substrate.

a discrete state-space model is built. Therefore a continuous state-space model is established first and a discretisation using zero order hold (zoh) is applied afterwards. The estimated power losses P_{loss} and the substrate temperature T_c are used as input parameters and outputs are the junction temperature estimations for IGBTs and power diodes. The temperatures of the thermal capacities are used as state-variables x_1 to x_4.

The state equations can be deduced from the thermal network using *Kirchhoff's* circuit laws:

$$\frac{dx_1}{dt} = -\frac{1}{C_{th1}R_{th1}}x_1 + \frac{1}{C_{th1}R_{th1}}x_2 + \frac{1}{C_{th1}}P_{loss} \quad (5)$$

$$\frac{dx_2}{dt} = \frac{1}{C_{th2}R_{th1}}x_1 - \frac{R_{th1}+R_{th2}}{C_{th2}R_{th1}R_{th2}}x_2 + \frac{1}{C_{th2}R_{th2}}x_3 \quad (6)$$

$$\frac{dx_3}{dt} = \frac{1}{C_{th3}R_{th2}}x_2 - \frac{R_{th2}+R_{th3}}{C_{th3}R_{th2}R_{th3}}x_3 + \frac{1}{C_{th3}R_{th3}}x_4 \quad (7)$$

$$\frac{dx_4}{dt} = \frac{1}{C_{th4}R_{th3}}x_3 - \frac{R_{th3}+R_{th4}}{C_{th4}R_{th3}R_{th4}}x_4 + \frac{1}{C_{th4}R_{th4}}T_c \quad (8)$$

As the junction temperature is the only output of the system, the output equation is noted as $T_j = x_1$.

This continuous state-space representation can be transformed into matrix notation, using a system matrix A , an input matrix B, an output matrix C and a feed-through matrix D. However, it does not contain additional information and thus is not written here.

The discrete state-space representation is denoted as:

$$\underline{x}(k+1) = A_d \cdot \underline{x}(k) + B_d \cdot \underline{u}(k) \quad (9)$$

and the output equation

$$\underline{y}(k) = C \cdot \underline{x}(k) + D \cdot \underline{u}(k) \quad (10)$$

To convert the continuous state-space into a discrete one sampled with sampling time t_s, following equations are used:

$$A_d = e^{(A \cdot t_s)} \quad (11)$$

$$B_d = e^{(A \cdot t_s - I)} \cdot A^{-1} \cdot B \quad (12)$$

To estimate the junction temperatures of all semiconductors in the module, several state-space models are used.

III. Active Thermal Control

The control structure and integration of an active thermal controller into an actual system is outlined first. The algorithm of the active thermal control is presented afterwards.

A. Active thermal control structure

It is assumed that a standard control structure like voltage or field oriented cascaded control is used. Now it is extended with an electro-thermal-model consisting of a device model, a losses model and a thermal model and a thermal control as shown in Fig. 3. The physical system provides measurements of the output current i_c, the dc link voltage v_{dc} and a low-bandwidth measurement of the substrate temperature T_c in the IGBT module. In this figure a reference voltage v_{ref} is generated by a general closed-loop current control. Its input i_c^* is the current reference. The required gate signals are created

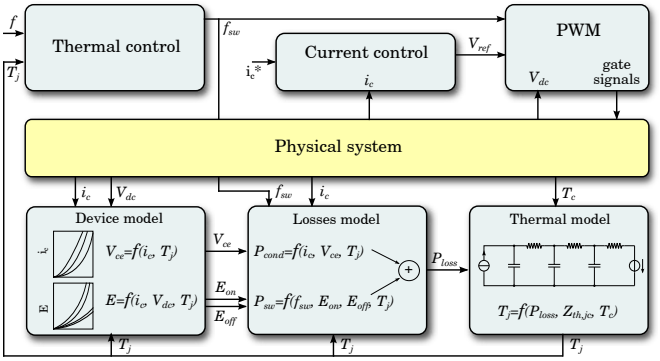

Fig. 3. Block scheme of the thermal control system.

in a pulse-width-modulator (PWM), using v_{ref}, v_{dc} and the switching frequency f_{sw}. This system is extended by the thermal control, which provides the switching frequency f_{sw} to the PWM and the losses model. The thermal control uses the online junction temperature estimations of the module's semiconductors T_j and the fundamental frequency f. These temperature estimations are provided by the electro-thermal model. The temperature dependencies in the model are satisfied with a feedback of the estimated temperature.

B. Active thermal control algorithm

The purpose of the algorithm is to detect thermal cycles and react in order to reduce their magnitudes. For the detection, a criterion for the thermal cycle amplitude ΔT_j is necessary. It is based on the junction temperature estimation T_j and its average value $T_{j,avg}$.

$$\Delta T_j = T_{j,avg} - T_j \quad (13)$$

This is displayed in Fig. 4(a). Positive values of ΔT_j indicate thermal cycles below the average temperature whereas negative values indicate thermal cycles over it. The average is created using a low-pass filter with a time constant adjusted to maximum length of a thermal cycle that has to be reduced by the thermal controller (i.e. $\tau = 60\,\mathrm{s}$). Just as T_j, the value of $T_{j,avg}$ is updated every sample time. Thus, ΔT_j is also available to the thermal control at every sampling period. A hysteresis controller is used to react on the detected thermal cycle amplitude. The switching frequency is changed according to the amplitude of thermal cycles between given values. The higher this amplitude is, the more losses have to be added in order to compensate the thermal cycle, so a higher switching frequency is selected. When the cycle ends, its amplitude vanishes and the switching frequency is reset to its minimum value. To prevent the controller from fast toggling between two switching frequencies, a sufficient hysteresis is used. Fig. 4(b) shows the hysteresis diagram.

The hysteresis points ΔT_{j1} to ΔT_{j4} have to be set reasonable for an effective operation of the hysteresis controller. For the given definition of ΔT_j, high values have to be compensated with an incremental of the power losses. For best results, the maximal amplitude of thermal cycles that may occur $\Delta T_{j,max}$ has to be identified e.g. by experiment.

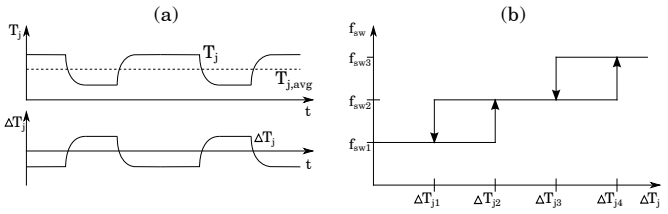

Fig. 4. Thermal cycle amplitude calculation (a) and hysteresis controller diagram (b).

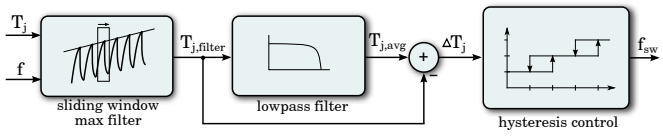

Fig. 5. Active thermal control block diagram.

Next the hysteresis points are distributed inside the interval $[0\ \Delta T_{j,max}]$. A definition that proved good results in practice is given as $\Delta T_{j1} = 0.15 \cdot \Delta T_{j,max}$, $\Delta T_{j2} = 0.25 \cdot \Delta T_{j,max}$, $\Delta T_{j3} = 0.4 \cdot \Delta T_{j,max}$ and $\Delta T_{j4} = 0.5 \cdot \Delta T_{j,max}$. A different empirical definition is given in [15].

A problem to deal with is the temperature ripple. It is not ensured that the temperature ripple in the junction temperature estimation caused by the fundamental frequency is not influencing the thermal controller. For the thermal cycle amplitude determination, it might happen that the temperature ripple of T_j is crossing the hysteresis control threshold, if the thermal cycling amplitude is already close to it. Also, the maximum value of the temperature ripple is of interest to determine the actual thermal cycle amplitude that acts in the chip. Thus, an additional filtering of the temperature input is done. The temperature ripple in the estimation can be removed most effectively, when the fundamental frequency f is known. This is the case, when the current reference for the current controller is computed in the same hardware and can otherwise be achieved by the use of a phase-locked-loop (PLL). Therefore, a sliding window maximum filter is applied. The window size is adjusted to the fundamental period and the end of the window is aligned with the latest sampled value. The filter output $T_{j,filter}$ is the maximum junction temperature within the last fundamental period, thus basically its peak value. The sliding window maximum filter adds a time delay to the control system, which effects its reaction time. As the thermal time constant is much larger than that of the filter, it is negligible. The active thermal control algorithm diagram is shown in Fig. 5.

IV. Experimental Results

First, hardware and measurement equipment data are given then experimental results are presented.

A. Experimental setup and measurement

The experimental validation is done on a single-phase two-level dc/ac inverter in H-bridge topology. A *Danfoss 25H1200T* three-phase inverter IGBT module ($i_{max} = 25\,\mathrm{A}$, $v_{dc,max} = 1200\,\mathrm{V}$) is used. An open module without the use of isolating gel filling is provided by the manufacturer. This allows direct temperature measurements on the chips but decreases the isolation voltage below the rated values. The power electronic part of the setup is shown in Fig. 6. For power input a $10\,\mathrm{kW}$ dc power supply is used. The load is ohmic-inductive. The control is implemented on a *dSPACE DS1006* processor board.

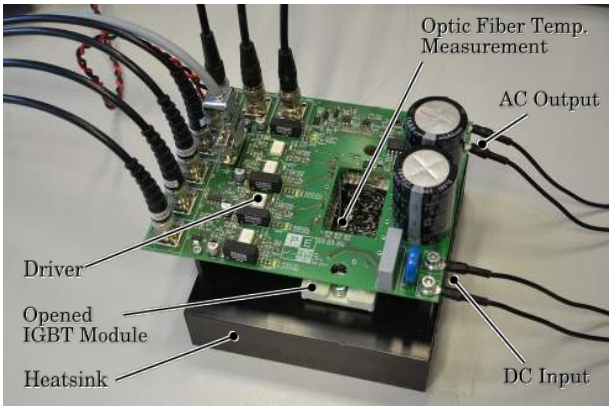

Fig. 6. Power electronic part of the setup used for experimental validation.

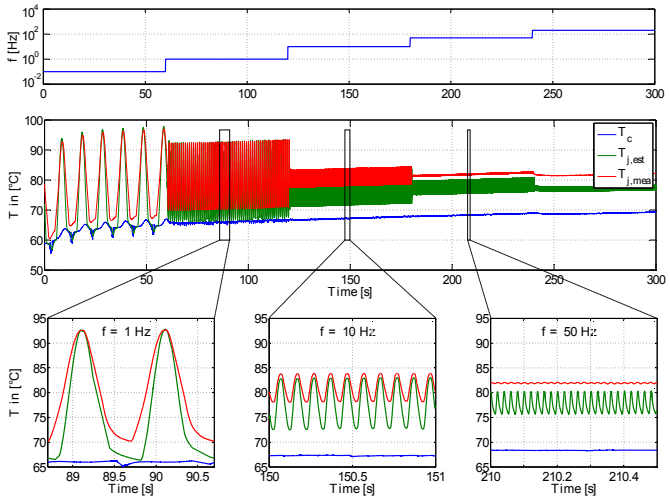

Fig. 7. Comparison of estimated and measured junction temperature. Variation of the fundamental frequency. Sinusoidal output current is controlled to $\hat{i} = 10\,\mathrm{A}$, dc voltage $v_{dc} = 270\,\mathrm{V}$, fixed switching frequency $f_{sw} = 20\,\mathrm{kHz}$.

For junction temperature measurement a optic fiber sensor is used that utilizes the temperature-dependency of GaA crystal bandgap. The response time is rated $5\,\mathrm{ms}$ and accuracy is rated $\pm 0.8\,\mathrm{K}$.

B. Validation of electro-thermal model

The temperature estimation provided by the electro-thermal model is compared to a direct measurement. Therefore, a variation of the fundamental frequency is done, while output power and switching frequency are fixed. The fundamental frequency f is changed to values of $0.1\,\mathrm{Hz}$, $1\,\mathrm{Hz}$, $10\,\mathrm{Hz}$, $50\,\mathrm{Hz}$ and $200\,\mathrm{Hz}$ in periods of $60\,\mathrm{s}$ to achieve steady-state in each test. The results are shown in Fig. 7. Estimation and

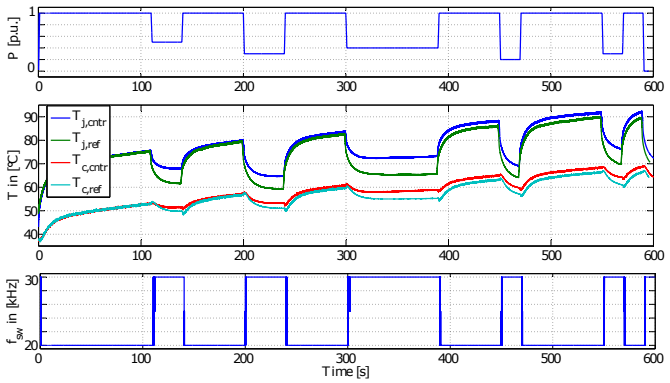

Fig. 8. Measured junction and case temperatures with and without the use of active thermal control for crane application. Output current is controlled to fit $\hat{i} = 10\,\mathrm{A}$ times the mission profile, fundamental frequency $f = 50\,\mathrm{Hz}$, dc voltage $v_{dc} = 400\,\mathrm{V}$.

TABLE I
THERMAL CYCLE AMPLITUDES AND NUMBER OF CYCLES TO FAILURE

	$i=1$	$i=2$	$i=3$	$i=4$	$i=5$
$\Delta T_{j,ref,i}$	13.7 K	20.8 K	18.6 K	21.3 K	20.4 K
$N_{f,ref,i}$	$1.1 \cdot 10^9$	$1.2 \cdot 10^8$	$2.2 \cdot 10^8$	$1.1 \cdot 10^8$	$1.4 \cdot 10^8$
$\Delta T_{j,cntr,i}$	7.3 K	15.1 K	11.0 K	18.6 K	15.8 K
$N_{f,cntr,i}$	$2 \cdot 10^{10}$	$6.6 \cdot 10^8$	$3.5 \cdot 10^9$	$2.2 \cdot 10^8$	$5.2 \cdot 10^8$

measurement are in a good match for the low fundamental frequencies of 0.1 Hz and 1 Hz. A deviation in both, mean value and thermal cycling amplitude is rising with increasing fundamental frequencies. An explanation can be found in the structure and parameters of the thermal network as well as in the used sensors and measurement. An error in the loss estimation is less likely as only the fundamental frequency is changed which has little influence on the losses. In the used model the direct heat transfer between collateral semiconductors is neglected. Thermal parameters have not been given by the manufacturer for the used module and were taken from the datasheet of a similar IGBT module. The response of the temperature sensor limits the measurements for high frequencies. Therefore, for these frequencies neither validation nor disproof of the temperature estimation is achieved.

C. Active thermal control in crane application

A mission profile of a 10 minutes crane or elevator application which is changing between holding and lifting is used. A similar profile is applied for a conveyor band with changing load. Temperatures are measured with and without the use of active thermal control. Results are shown in Fig. 8.

A reduction of the thermal cycle amplitudes is achieved for both, junction and case temperatures. Besides a slight increment of the average temperature has taken place for both measurements. The thermal cycle amplitudes are shown in Table I for the five occurring thermal cycles of Fig. 9. To evaluate the impact of the thermal control, the Coffin-Manson model and a variation of Miner's rule are applied. The number of cycles to failure N_f is noted for each thermal cycle using data and extrapolation from Fig. 9. Subsequent, Miner's Rule

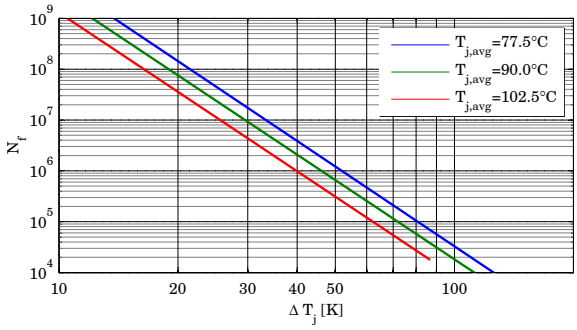

Fig. 9. Number of cycles to failure N_f in dependency of thermal cycle amplitude ΔT_j and average junction temperatures $T_{j,avg}$ for IGBT4 modules. Data taken from [5].

[9] is used to compute the amount of cumulative damage taken by one run of the profile for both curves, fixed c_{ref} and thermal controlled c_{cntr} switching frequency:

$$c_{ref} = \sum_{i=1}^{5} \frac{n_i}{N_{f,ref,i}} = 3.00 \cdot 10^{-8} \tag{14}$$

$$c_{cntr} = \sum_{i=1}^{5} \frac{n_i}{N_{f,cntr,i}} = 8.32 \cdot 10^{-9} \tag{15}$$

When the cumulative damage reaches 1, the device fails according to Miner's Rule. The number of cycles is set to $n_i = 1,\ \forall i$, as every thermal cycle amplitude occurs only once in the profile. To give a more descriptive result on the impact of lifetime, the amount of cumulative damage is converted to the number of repetitions of the given mission profile until failure:

$$N_{f,profile,ref} = \frac{1}{c_{ref}} = 3.3 \cdot 10^7 \tag{16}$$

$$N_{f,profile,cntr} = \frac{1}{c_{cntr}} = 1.2 \cdot 10^8 \tag{17}$$

As a result, the lifetime of the module can be extended by a factor more than 3 using the proposed active thermal control algorithm on the given mission profile. The enhanced lifetime saves costs and materials due to reduced replacement parts, maintenance and loss of production. The drawbacks are additional losses resulting in higher average temperatures and additional energy consumption costs in operation.

D. Active thermal control in electric vehicle

The mission profile of a 20 minutes urban drive of a small electric vehicle without energy recuperation is run on the experimental setup. Junction temperatures are measured with and without the use of active thermal control. The results are shown in Fig. 10. Again, a reduction of the thermal cycle amplitudes is achieved for both, junction and case temperatures. Besides an increment of the average temperature occurred for both measurements. During acceleration after stop low fundamental frequencies and high currents occur resulting in temperature swings. These fundamental frequency thermal cycles can not be reduced with the proposed thermal control

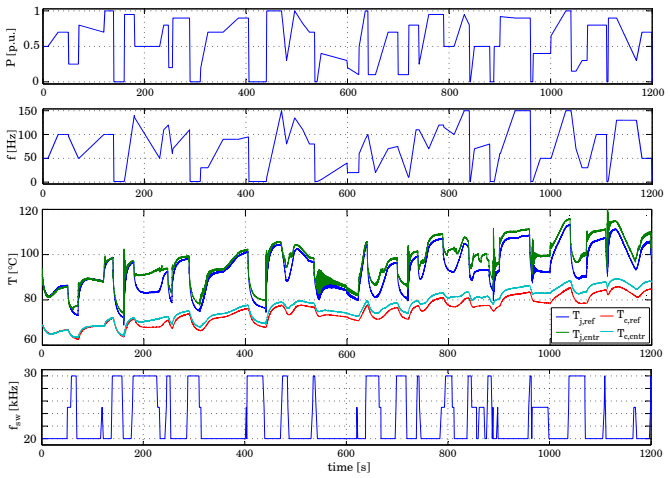

Fig. 10. Electric vehicle temperature profile with and without active thermal control. Output current is controlled to fit $\hat{i} = 12\,\mathrm{A}$ times the mission profile and given fundamental frequency, dc voltage $v_{dc} = 400\,\mathrm{V}$, uncontrolled switching frequency $f_{sw} = 20\,\mathrm{kHz}$.

structure for the given H-bridge setup. During low load on one IGBT, the opposite IGBT has a high load in a fundamental period. Therefore, an increment of the switching frequency would lead to increasing temperatures in both IGBTs and the thermal cycle amplitude in the opposite IGBT would increase.

The overall reduction of thermal cycles is less distinct than in the previous crane application. Since the electric vehicle urban drive mission profile includes segments of no power, the proposed thermal control can only add a slight amount of additional losses in these segments when increasing the switching frequency. In changes from full to partial load, thermal cycles can be reduced more efficient as the thermal control has a stronger effect on the losses.

V. Conclusion

A reduction of thermal cycles in power electronic modules can be achieved for different applications using active thermal control. This is also possible by only increasing the switching frequency compared to the not thermal controlled reference. A possibility for online junction temperature estimation without additional sensors has been introduced and applied for active thermal control. This allows a subsequent adoption of temperature control without changes to the system hardware.

Experimental verification provided that the accuracy of the temperature estimation is in good match with the measurement for fundamental frequencies up to 10 Hz. Higher frequencies could not be validated. Experimental comparisons of temperature profiles with and without active thermal control showed a possible reduction of thermal cycles amplitudes that can increase the module's lifetime by a factor of 3 according to the Coffin-Manson model and Miner's accumulated damage rule.

Acknowledgment

The research leading to these results has received funding from the Gesellschaft für Energie und Klimaschutz Schleswig-Holstein GmbH (EKSH) doctoral studies grant.

References

[1] R. Teodorescu, M. Liserre, and P. Rodriguez, *Grid converters for photovoltaic and wind power systems*. John Wiley & Sons, 2011, vol. 29.

[2] J. Lemmens, P. Vanassche, and J. Driesen, "Optimal control of traction motor drives under electrothermal constraints," *Emerging and Selected Topics in Power Electronics, IEEE Journal of*, vol. 2, no. 2, pp. 249–263, June 2014.

[3] H. Wang, M. Liserre, and F. Blaabjerg, "Toward reliable power electronics: Challenges, design tools, and opportunities," *Industrial Electronics Magazine, IEEE*, vol. 7, no. 2, pp. 17–26, June 2013.

[4] H. Wang, M. Liserre, F. Blaabjerg, P. de Place Rimmen, J. Jacobsen, T. Kvisgaard, and J. Landkildehus, "Transitioning to physics-of-failure as a reliability driver in power electronics," *Emerging and Selected Topics in Power Electronics, IEEE Journal of*, vol. 2, no. 1, pp. 97–114, March 2014.

[5] A. Wintrich, U. Nicolai, W. Tursky, and T. Reimann, "Semikron, application manual power semiconductors," *Ilmenau: ISLE*, 2011.

[6] C. Busca, R. Teodorescu, F. Blaabjerg, S. Munk-Nielsen, L. Helle, T. Abeyasekera, and P. Rodriguez, "An overview of the reliability prediction related aspects of high power igbts in wind power applications," *Microelectronics Reliability*, vol. 51, no. 9, pp. 1903–1907, 2011.

[7] B. Ji, V. Pickert, W. Cao, and B. Zahawi, "In situ diagnostics and prognostics of wire bonding faults in igbt modules for electric vehicle drives," *Power Electronics, IEEE Transactions on*, vol. 28, no. 12, pp. 5568–5577, Dec 2013.

[8] A. Volke and M. Hornkamp, *IGBT modules: technologies, driver and application*, 2nd ed. Infineon Technologies AG, 2012.

[9] I. Kovacevic, U. Drofenik, and J. Kolar, "New physical model for lifetime estimation of power modules," in *Power Electronics Conference (IPEC), 2010 International*, June 2010, pp. 2106–2114.

[10] V. Smet, F. Forest, J.-J. Huselstein, F. Richardeau, Z. Khatir, S. Lefebvre, and M. Berkani, "Ageing and failure modes of igbt modules in high-temperature power cycling," *Industrial Electronics, IEEE Transactions on*, vol. 58, no. 10, pp. 4931–4941, Oct 2011.

[11] T. Herrmann, M. Feller, J. Lutz, R. Bayerer, and T. Licht, "Power cycling induced failure mechanisms in solder layers," in *Power Electronics and Applications, 2007 European Conference on*, Sept 2007, pp. 1–7.

[12] B. Ji, X. Song, E. Sciberras, W. Cao, Y. Hu, and V. Pickert, "Multi-objective design optimization of igbt power modules considering power cycling and thermal cycling," *Power Electronics, IEEE Transactions on*, vol. 30, no. 5, pp. 2493–2504, May 2015.

[13] X. Wang, A. Castellazzi, and P. Zanchetta, "Regulated cooling for reduced thermal cycling of power devices," in *Power Electronics and Motion Control Conference (IPEMC), 2012 7th International*, vol. 1, June 2012, pp. 238–244.

[14] D. Murdock, J. Torres, J. Connors, and R. Lorenz, "Active thermal control of power electronic modules," *Industry Applications, IEEE Transactions on*, vol. 42, no. 2, pp. 552–558, March 2006.

[15] M. Weckert and J. Roth-Stielow, "Lifetime as a control variable in power electronic systems," in *Emobility - Electrical Power Train, 2010*, Nov 2010, pp. 1–6.

[16] J. Lemmens, J. Driesen, and P. Vanassche, "Dynamic dc-link voltage adaptation for thermal management of traction drives," in *Energy Conversion Congress and Exposition, 2013 IEEE*, Sept 2013, pp. 180–187.

[17] C. Sintamarean, H. Wang, F. Blaabjerg, and F. Iannuzzo, "The impact of gate-driver parameters variation and device degradation in the pv-inverter lifetime," in *Energy Conversion Congress and Exposition (ECCE), 2014 IEEE*, Sept 2014, pp. 2257–2264.

[18] K. Ma, M. Liserre, and F. Blaabjerg, "Reactive power influence on the thermal cycling of multi-mw wind power inverter," *Industry Applications, IEEE Transactions on*, vol. 49, no. 2, pp. 922–930, March 2013.

[19] M. Andresen, G. Buticchi, J. Falck, M. Liserre, and O. Muehlfeld, "Active thermal management for a single-phase h-bridge inverter employing switching frequency control," in *PCIM Europe 2015; Proceedings of*, May 2015, pp. 1–8.

[20] L. Coffin Jr, "A study of the effects of cyclic thermal stresses on a ductile metal," *Trans. ASME*, vol. 76, pp. 931–950, 1954.

[21] N. Baker, M. Liserre, L. Dupont, and Y. Avenas, "Junction temperature measurements via thermo-sensitive electrical parameters and their application to condition monitoring and active thermal control of power converters," in *Industrial Electronics Society, IECON 2013 - 39th Annual Conference of the IEEE*, Nov 2013, pp. 942–948.